ELSEVIER

Journal of Magnetism and Magnetic Materials 200 (1999) 552–570

Journal of magnetism and magnetic materials

www.elsevier.com/locate/jmmm

Exchange anisotropy — a review

A.E. Berkowitz[a,*], Kentaro Takano[b]

[a]Department of Physics and Center for Magnetic Recording Research, University of California at San Diego, La Jolla, CA 92093-0401, USA
[b]IBM Almaden Research Center, 650 Harry Rd., San Jose, CA 95120, USA

Received 12 March 1999

Abstract

Exchange anisotropy refers to the magnetic manifestations of an exchange coupling at the interface between two different magnetically ordered systems. Of particular current technological interest is the unidirectional anisotropy, or 'exchange-bias' field produced in a ferromagnetic film that is coupled to an appropriate antiferromagnetic film. Experimental characterization and theoretical models are discussed for these types of bilayers for a variety of metallic and oxide film couples.

Keywords: Exchange anisotropy; Interfaces; Thin films

1. Introduction and background

In 1956, Meiklejohn and Bean (M–B) reported [1,2] '*A new type of magnetic anisotropy has been discovered which is best described as an exchange anisotropy. This anisotropy is the result of an interaction between an antiferromagnetic material and a ferromagnetic material*'. In the more than 40 years since its discovery, the phenomenon of exchange anisotropy has become the basis for an important application in information storage technology, with a high current level of world-wide research and development activities. However, it has only been within the last decade or so that a basic, quantitatively predictive, understanding of exchange anisotropy has begun to be developed significantly beyond the initial seminal model presented by M–B. The relatively slow pace of rigorous modeling is due primarily to the fact that exchange anisotropy is the result of an interfacial exchange interaction between ferromagnetic (FM) and antiferromagnetic (AFM) materials, and only recently have the required experimental and analytical tools for dealing with interfacial behavior at the atomic level become available. This review will discuss primarily those research results which, at present, seem to offer the most insight into a reliable model. Previous reviews in which exchange anisotropy is considered in significant detail are found in Refs. [3–5].

1.1. Meiklejohn and Bean's research

M–B's discovery was initiated by the observation that the hysteresis loop below room temperature of a sample of nominal Co nanoparticles was shifted along the field axis after cooling in an applied field.

* Corresponding author. Tel.: +1-858-534-5627; fax: +1-858-534-2720.
E-mail address: aberkowitz@ucsd.edu (A.E. Berkowitz)

0304-8853/99/$ - see front matter
PII: S0304-8853(99)00453-9

It was subsequently established that the particles had been partially oxidized to CoO which is an AFM. Thus, the particles could be considered to consist of a core of single-domain Co with a shell of AFM CoO. M–B described how the exchange interaction across the interface between the FM Co and the AFM CoO could produce the shifted hysteresis loop and the other unique manifestations of exchange anisotropy. The initial papers of M–B [1,2], together with the review by Meiklejohn [3], anticipated virtually all the features of subsequent experimental observations and models for exchange anisotropy.

Fig. 1a shows hysteresis loops at 77 K of a compact of fine partially oxidized Co particles (10–100 nm). The shifted loop (curve 1) was measured after cooling in a field of 10 kOe; the symmetric loop (curve 2) was measured after cooling in zero field. M–B showed that the loop shift was equivalent to the assumption of a unidirectional anisotropy energy in the expression for the free energy at $T = 0$ K of a single-domain spherical particle with uniaxial anisotropy, aligned with its easy axis in the direction of the field, H, which is applied anti-parallel to the particle's magnetization, M_s, i.e.,

$$F = HM_s \cos \Theta - K_u \cos \Theta + K_1 \sin^2 \Theta,$$

where Θ is the angle between the easy direction and the direction of magnetization, and K_u and K_1 are the unidirectional and uniaxial anisotropy energy constants, respectively. Solutions of this equation are readily expressed in terms of an effective field

$$H' = H - K_u/M_s,$$

which gives the hysteresis loop displaced by K_u/M_s, on the H-axis. Thus, an explanation of the loop shift is equivalent to explaining the unidirectional anisotropy.

AFM materials, such as CoO, magnetically order below their Néel temperatures, T_N, with the spins of the Co^{2+} cations parallel to each other on (1 1 1) planes, and with anti-parallel spin directions in alternate (1 1 1) planes, i.e., zero net moment. However, at the interface with a FM, there are localized net moments which arise from several sources (discussed in the Models and theories section). The most obvious case is where there are AFM grains with parallel spin planes at the interface as depicted in Fig. 2. Alternatively, even in AFM grains with compensated interfacial spin planes, there can be unequal numbers of parallel and anti-parallel spins at the surface of the grain, due to grain size, shape, or roughness. These various origins of localized net

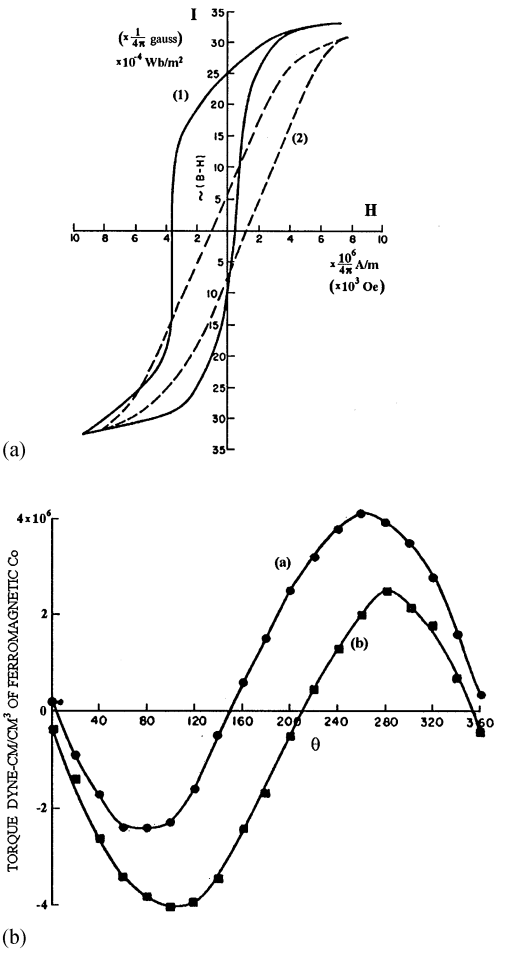

Fig. 1. (a) Hysteresis loops at 77 K of partially oxidized Co particles. Curve (1) shows the resulting loop after cooling the compact in a 10 kOe field. Curve (2) shows the loop when cooled in zero field. (b) Torque curves on partially oxidized Co particles cooled in a field to 77 K, where θ is the angle between the cooling field axis and the direction of the measuring field. Curves a and b in (b) are for counterclockwise and clockwise rotations, respectively. From Refs. [1,2].

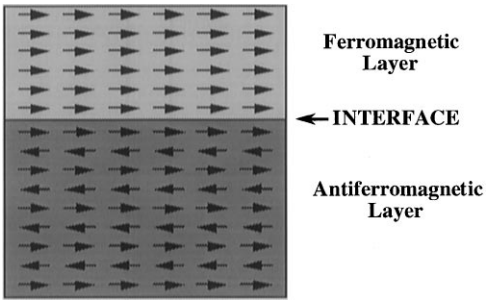

Fig. 2. Schematic of the *ideal* FM/AFM interface. The FM and AFM layers are single crystal and epitaxial with an atomically smooth interface. The interfacial AFM spin plane is a fully uncompensated spin plane. For this ideal interface, the calculated value of the full interfacial energy density is about two orders of magnitude larger than the experimentally observed values.

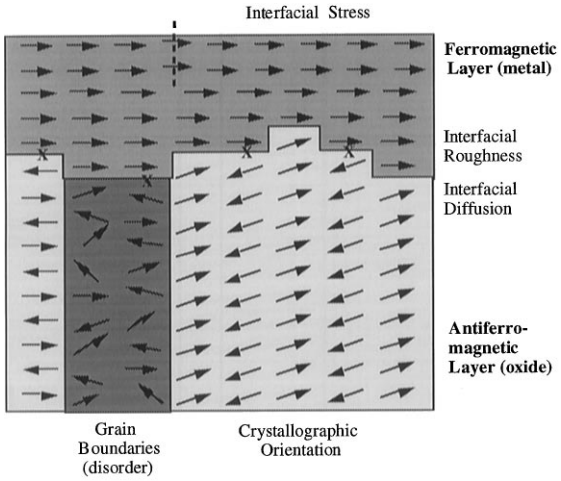

Fig. 3. Interfacial complexities of a polycrystalline FM(metal)/AFM(oxide) interface. In this figure, the interfacial spins prefer to align ferromagnetically. The X marks identify the frustrated exchange bonds, i.e. the interfacial spins that are coupled antiferromagnetically. The interfacial region can have a high degree of stress since metals and oxides often have very different lattice parameters. Dislocations (represented by the dashed line) can form during film growth to relieve the stress.

AFM moments are depicted in Fig. 3. Since the FM is ordered at its Curie temperature, T_C, which is greater than T_N of the AFM, a field applied to coupled FM–AFM systems at $T > T_N$ will align the FM magnetization in the field direction, while the AFM spins remain paramagnetic. As the temperature is lowered through T_N, the ordering net localized AFM spins will couple to the aligned FM spins, sharing their general spin direction. For high AFM magnetocrystalline anisotropy, if the interfacial AFM spins are strongly coupled to the AFM lattice, they will not be substantially rotated out of their alignment direction by fields applied at temperatures below T_N. This is also a consequence of the fact that the generally compensating anti-parallel arrangement of the AFM spins does not result in a strong torque on the spin system when a field is applied (i.e., low susceptibility). However, since the localized uncompensated AFM spins are coupled to FM spins at the interface, they exert a strong torque on these FM spins, tending to keep them aligned in the direction of the cooling field, i.e., a unidirectional anisotropy. This model explains the shift in curve 1 in Fig. 1a, for the field-cooled particles. When the particles are cooled in zero field, there is still a unidirectional bias in each particle, but since the moments of the particles are randomly arranged, there is no net bias, and curve 2 in Fig. 1a is symmetric.

M–B anticipated and considered all of the exchange anisotropy issues dealt with in more detail below. These include: (a) how the relative strengths of the interfacial exchange coupling and the AFM magnetocrystalline anisotropy determine whether a unidirectional anisotropy dominates, or whether the AFM spin system is switched as the FM rotates, producing high-field rotational hysteresis; (b) how walls in either the FM or AFM can influence the observed behavior; (c) how the field-cooling parameters influence the resulting unidirectional anisotropy; and (d) the temperature dependence of the bias field.

1.2. Other early work

The 1962 review by Meiklejohn [3] discusses a number of two-phase systems in which various properties could plausibly be attributed to exchange anisotropy. These include not only FM–AFM, but also ferrimagnetic–AFM, and ferrimagnetic–FM combinations. Rotational hysteresis (W_R) is the integrated displacement of torque curves measured with the field rotated in the

plane of the sample in clockwise and counterclockwise directions, as shown in Fig. 1b. Meiklejohn presented an expanded model for the existence of W_R in FM–AFM systems for fields $> 2K_1/M_s$ of the FM. Above T_N of the CoO coating, the single-domain particles of Co with uniaxial anisotropy were shown to exhibit W_R only for fields between K_1/M_s and $2K_1/M_s$. However, with an AFM-ordered CoO shell, Co particles have finite W_R in fields $H \gg 2K_1/M_s$. Meiklejohn showed this occurs when the exchange anisotropy constant, $K_u > K_{AFM}$. This high field W_R is due to the discontinuous switching of the AFM spin system twice each cycle as the FM is rotated 360° by the applied field. This is a consequence of the torque exerted on the AFM spin system by the FM to which it is coupled. The magnitude of W_R depends on K_u/K_{AFM}, and on the AFM thickness (i.e., net AFM magnetocrystalline energy). The additional interaction of the AFM spin system with the applied field was described by Berkowitz and Greiner [6].

Meiklejohn called attention to the ideal manifestations of unidirectional anisotropy in the atomically disordered Mn alloys investigated by Kouvel [7]. In these alloys, the Mn atoms have either FM or AFM exchange interactions, depending on whether they are nearest or next-nearest neighbors, respectively. Accordingly, Kouvel ascribed the unidirectional anisotropy to adjacent exchange coupled FM and AFM regions which were present as localized composition fluctuations. Satoh et al. [8] used high field measurements to determine the magnitude of the coupling field in Mn–Ni alloys of this type.

Néel [9] considered in detail the behavior of partially oxidized FM films in which the oxide was AFM (e.g., Co–CoO, Ni–NiO), and was assumed to be in the form of small grains. He discussed the issues of high field W_R in these films in much the same spirit as Meiklejohn did for the partially oxidized particles. Néel focused particularly on the behavior of these films under repetitive cycling of the field. He described how the loop shift, and its dependence on the amplitude of the cycled applied field, varied with the number of field cycles. He distinguished among three types of hysteresis loss: AC loss, where the field varies between $+H$ and $-H$; rotational hysteresis, in which a fixed field is rotated through complete cycles; and oscillatory hysteresis, in which a fixed field is rotated between two fixed directions. Néel also considered the still-open question of the nature of the exchange interaction at the FM–AFM interface on an atomic level. Yelon's review [5] includes a useful summary of Néel's work in this area. Charap and Fulcomer [10,11] extended the consideration of the magnetization dynamics of this type of oxidized film with experimental observations and models. They observed viscous domain wall motion, as well as frequency- and temperature-dependent loop displacements which they modeled by considering thermally induced fluctuations of the spin systems of the small AFM grains coupled to the FM film. Their papers contain references to the other significant investigations in similar systems. Bostanjoglo et al. [12,13] reported some of the first Lorentz micrographs of domain wall structures taken at various stages of magnetization reversal in NiFe–NiFeMn couples after one or more field cycles. They concluded that the decreasing loop shift with progressive field cycling was accompanied by a rotation of the unidirectional anisotropy axis by 90°. The investigations noted above point to a growing awareness of the extraordinary complexity and the significance of the chemical and magnetic structure at the FM–AFM interface.

2. More recent investigations

During the past several decades, the pace of activity involving FM–AFM exchange couples has greatly increased. The reason is that the effective bias field, H_E, on a FM thin film produced by the interfacial exchange with an AFM film, has found an extremely useful application in the information storage industry. The digital data in current high-density magnetic storage disks is sensed by read-heads which employ thin FM film devices whose resistance varies with the magnitude and direction of the stray fields above the stored bits [14]. This is the phenomenon of *magnetoresistance* (MR). To linearize the bipolar MR signal, and to minimize the noise produced by discontinuous jumps of domain walls (Barkhausen noise), the FM films must be biased by a magnetic field. Coupling the FM

film to an AFM film provides a substantial fraction of the required bias in all current high-density read-heads. All of the initial AFM films used for this purpose were metallic Mn alloys, particularly Fe–Mn. Recently, read-heads using the more robust insulating AFM bias films such as NiO have been appearing. Since the exchange interactions and spin structures are quite different in metallic and insulating AFM materials, the behavior of exchange couples with these two types of AFMs are considered separately below.

By the mid-1970s virtually all of the most significant static and dynamic features of FM–AFM exchange coupling had been recognized, and plausible qualitative models had been developed for a number of issues. What was lacking, and is still missing, was adequate characterization of the chemical states and the exchange interactions at the FM–AFM interface *on an atomic scale*. Until this extremely complex information becomes available, there can be no rigorously reliable explanations for the salient features of exchange anisotropy in FM–AFM couples. Therefore, the papers discussed below were primarily selected with the hope that they offered significant clues to a basic understanding by virtue of their (i) careful sample preparation; (ii) useful interfacial characterization; or (iii) unique exchange properties. In all these cases, the FM–AFM exchange couples are thin films.

2.1. Exchange couples with insulating AFM films

Almost all the reported investigations with insulating AFMs involve the monoxides NiO, CoO, and $Ni_xCo_{(1-x)}O$. An important exception is FeF_2. Detailed work with other oxides such as α-Fe_2O_3 and orthoferrites are preliminary and still in progress. The monoxides have an FCC structure above T_N, with a slight distortion below T_N [15]; rhombohedral contraction along $\langle 1\,1\,1\rangle$ in NiO, tetragonal contraction along $\langle 1\,0\,0\rangle$ in CoO. The bulk T_N for CoO is 293 K; for NiO, it is 525 K. For $Ni_xCo_{(1-x)}O$, T_N varies linearly with x [16]. Above T_N, the monoxides are paramagnetic. Below T_N, they order with parallel spins on (1 1 1) planes, and with anti-parallel spin directions on adjacent planes (i.e., the spins of next nearest neighbors along $\langle 1\,0\,0\rangle$ are anti-parallel due to the superexchange interaction via an intervening oxygen atom). This is depicted in Fig. 4. The four different $\langle 1\,1\,1\rangle$ axes for spin ordering combined with the non-cubic distortions below T_N, make for a rich variety of AFM domain structures, which was described in detail by Roth and Slack [17–19]. An AFM domain is identified by its Néel axis, the direction along which the spins are either parallel or anti-parallel. Since it is difficult to prepare single-domain samples, it has not been possible to accurately measure the magnetocrystalline constants of the AFM monoxides. The spins can be rotated much more easily within the coherently magnetized (1 1 1) planes than out of these planes. Thus, two anisotropy constants can be identified, K_1 for rotation out of the (1 1 1) spin plane, and K_2 for rotation within this plane. The unquenched orbital momentum of Co^{2+} gives CoO a very high magnetocrystalline anisotropy. Kanamori has calculated $K_1 \approx 2.7\times10^8$ erg/cm^3 [20]. At 4.2 K, $K_2 < 2\times10^5$ was obtained [21]. For NiO, values reported for K_1 are 1 to 5×10^6 [22–25]; K_2 has been variously measured [26–29], and calculated [30] from 0.1 to $\sim$5% of K_1. Although there is considerable uncertainty as to the correct values of K_1 and K_2, there is no doubt that both are much higher for CoO than for NiO.

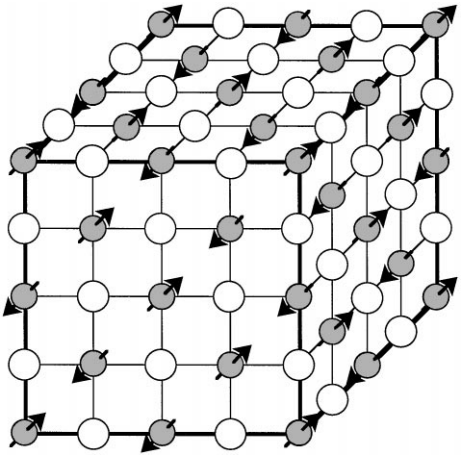

Fig. 4. Chemical and magnetic structure of $Ni_xCo_{(1-x)}O$ antiferromagnetic materials. The shaded spheres represent the magnetic metal atoms, and the unfilled spheres represent the oxygen atoms.

In a general sense, the recent (1990s) investigations of exchange couples with monoxide AFM and metallic FM films have served to confirm the initial suggestions of Meiklejohn, Bean, and Néel, albeit with more sensitive and refined experimental and analytical methods. The principal achievements have been: (1) demonstrating that the uncompensated AFM interfacial spin density determines H_E; (2) H_C increases with lower AFM anisotropy energies; (3) thermally activated aftereffects are frequently observed. Furthermore, a quantitatively predictive model for H_E has been developed for CoO-permalloy couples.

Carey and Berkowitz [31] reported the preparation, by reactive sputtering, of AFM films of CoO, NiO, and $Ni_xCo_{(1-x)}O$. When coupled to permalloy, the blocking temperatures, T_B (and, by inference, T_N also) of the $Ni_xCo_{(1-x)}O$ varied linearly with x from the CoO to the NiO values. H_E and H_C were determined as functions of x; for $x > 20$ vol%, H_E/H_C was > 1, a necessary condition for biasing read-heads. The same authors measured $H_E(T)$ of CoO–NiO superlattices exchange coupled to permalloy [32]. These data indicated a sufficiently strong exchange interaction at CoO–NiO interfaces such that when the superlattice repeat distance was $\leqslant 2$ nm, a single ordering temperature existed, and T_N was the same as an alloy with the same vol% of CoO and NiO. This was later confirmed by neutron diffraction [33]. $H_E(T)$ also depended on whether a CoO or NiO layer was adjacent to the permalloy. Generally, this work pointed to several potential options for control of $H_E(T)$. However, the definitive aspects of this work primarily focus on the magnetic ordering within the AFM. The results pertaining to exchange biasing are only suggestive since it still remains to model and establish definitively the AFM superlattices' effectiveness for exchange biasing.

Since the bulk T_N of CoO is approximately room temperature, and its magnetocrystalline anisotropy is high, CoO–FM is a very useful model system since magnetic characterization is conveniently performed using a SQUID magnetometer. A systematic study of polycrystalline CoO–permalloy exchange couples by Takano et al. [34,35] clearly demonstrated that the AFM interfacial uncompensated spin density determines H_E, independent of compensation considerations, and a model was developed that provided the first quantitative predictions of H_E for a given system. That work is discussed in detail below in the section on Models and Theories. It was demonstrated experimentally and analytically that the density of AFM uncompensated interfacial spins was inversely proportional to the average interfacial grain diameter. Although smaller interfacial grains produced higher H_E at low temperatures, H_E was significantly temperature dependent if the grain had a correspondingly small volume [36]. This is a consequence of the fact that the anisotropy energies of the AFM grains are proportional to their volumes; therefore, sufficiently small grains can be subject to thermally activated fluctuations of their spin systems, analogous to superparamagnetism in FM nanoparticles, but modified by the coupling to the FM. Accordingly, Martien et al. [37] showed that textured AFM $Co_{0.5}Ni_{0.5}O$ films in which the interfacial grain diameters were small but elongated normal to the interface, yielded increased H_E with minimal decrease in thermal stability.

Two investigations have emphasized the complex atomic scale chemical and spin distributions at the CoO interface with a FM material. Moran et al. [38] used bulk CoO (1 1 1) crystals which were mechanically roughened to various degrees. Permalloy was deposited on these surfaces, and H_E and H_C were measured after field-cooling from above T_N. H_E regularly increased with roughness, which seemed counterintuitive at the time, but is consistent with the quite plausible notion of an uncompensated spin density increasing with roughness. Spagna et al. [39] reported the properties of Co–CoO bilayers and Co–CoO–Co trilayers in which the CoO was formed by partially oxidizing the Co films. A depth profiling technique, using Auger electron spectroscopy in conjunction with 1 keV Ar^+ ion sputter etching, showed a linear decrease of both Co and oxygen over a distance of 2.3 nm from the 100% Co surface of a film that was initially 8 nm of Co. In spite of this strong evidence for a lack of a sharp interface, H_E was ≈ 1 kOe at 20 K. H_E vanished at ~ 150 K, presumably because the spin system in the non-uniform 2.3 nm oxide layer became thermally unstable. However, Abarra et al. [40] found T_N of a 2.3 nm film of CoO was

$\approx$270 K, and Takano [36] determined that T_b to be one-half T_N only in cases where the sizes of the oxide grains were extremely small — i.e., when deposited on cryogenically cooled substrates. The nature of the interfacial exchange interaction, whether superexchange or direct exchange, is not known at present. A start in elucidating this question was made by Takano and co-workers [36]. They deposited a number of different FM films on CoO underlayers, and measured the low-temperature H_E. A mean field analysis of these values permitted discrimination between direct and superexchange. At a metal–oxide interface, one might expect superexchange to dominate; however, the analysis suggested direct exchange as the limiting interfacial exchange.

In the exchange couples with CoO discussed above, the FM layer was a metal. Several important studies have been made in which CoO was coupled to Fe_3O_4, a ferrimagnet (FIM) which has two FM sublattices of unequal magnetization oriented antiparallel. The net magnetization of Fe_3O_4 vanishes at its Curie temperature, $T_C = 858$ K. Since the lattice constant of Fe_3O_4 is twice that of CoO, and the FCC oxygen lattice has very similar dimensions in both materials, they can be grown epitaxially. This was demonstrated by Terashima and Bando [41], who grew multilayers of CoO–Fe_3O_4 pairs with various film thicknesses and numbers of bilayer repeats, on (1 0 0) cleaved NaCl. X-ray structure analysis confirmed epitaxial growth for thicker ($\sim$5.0–10.0 nm) Fe_3O_4, with evidence of cation disorder in thinner films. A surprising result was the existence of a hysteresis loop shift for CoO(2.2 nm)–Fe_3O_4(9.0 nm) at room temperature, since such thin CoO was expected to be paramagnetic or at least superparamagnetic at that temperature.

van der Zaag et al. [42,43] have prepared epitaxial bilayers of CoO and Fe_3O_4 with (1 0 0) and (1 1 1) orientations. They examined the CoO thickness (t_{Co}) dependence of H_E and T_B. They found that T_B was $\approx T_N$ of CoO for $t_{Co} \geqslant 8.0$ nm. H_E(0 K) was maximum for 2.0 nm $< t_{Co} <$ 5.0 nm. Ijiri et al. [44,45] used neutron diffraction to investigate spin configurations in (0 0 1)[Fe_3O_4(10 nm)–CoO(30 nm)]$_{50}$ and [Fe_3O_4(10 nm)–CoO(10 nm)]$_{50}$ superlattices prepared by van der Zaag and Wolf. The most remarkable result was the observation, after field-cooling, that the CoO spins aligned perpendicular to the Fe_3O_4 net moment. The two samples also exhibited very high H_E (550 and 1300 Oe), H_C (6000 and 3200 Oe), and T_N (450 and 325 K), respectively. These values suggest a highly complex interfacial spin structure, with the likelihood of propagation of anomalous magnetic order throughout the superlattices, evidenced by the extension of the AFM coherence across the bilayers. Another possible factor might be the presence of ferrimagnetic Co-ferrite-like magnetic order, with an enormous magnetocrystalline anisotropy. Along these lines, Kleint et al. [46] found shifted loops in Fe_3O_4–$Co_xFe_{(3-x)}O_4$ bilayers, and ascribed H_E to the reversal of the softer Fe_3O_4 without changing the magnetization direction of the harder $Co_xFe_{(3-x)}$. This study emphasized the extremely complex interfacial magnetic structure.

The relatively high T_N of NiO makes it attractive for commercial applications. However, its low magnetocrystalline anisotropy (1) limits H_E, and (2) increases H_C, when the interfacial exchange exceeds the magnetic energy of the AFM grain. A number of studies have confirmed this behavior. Lee et al. [47] compared epitaxial NiO–NiFe bilayers prepared on (1 0 0), (1 1 0), and (1 1 1)MgO to polycrystalline NiO–NiFe. They also measured roughness. They concluded that texture did not play a significant role in determining H_E, but that roughness seemed to increase H_C. Han et al. [48] concluded that low interfacial roughness was the key to low H_C in NiO–$Ni_{81}Fe_{19}$ exchange couples, and that H_E was insensitive to texture. Michel et al. [49] compared the behavior of epitaxial (0 0 1) and polycrystalline NiO–NiFe bilayers. They found that the polycrystalline couples had larger H_E than the epitaxial ones. They suggested that a static surface anisotropy with reversible interfacial NiO spin dynamics could account for a large part of the observed behavior. However, they noted that the presence of high-field rotational hysteresis indicated some irreversible AFM spin dynamics. They also called attention to the possibility that the existence of interfacial roughness, stress, and domains in the AFM layer could produce frustration in the interfacial layer, a spin-glass like situation previously suggested by Stoecklein et al. [50] and

by Schlenker et al. [51]. Mössbauer studies by Takano and Parker [36] would tend to provide support for such a topologically disordered spin configuration. Their data suggest that the interfacial atoms occupy a variety of valence states and chemical environments. In a study of spin valves, Chopra et al. [52] used high-resolution TEM to show how the atomic structure of a NiO–Co interface varied with the O_2 sputtering pressure during reactive deposition of the NiO onto the Co film, and how the resulting pinning field reflected the interfacial structure. These authors emphasize that their pinning is primarily accomplished by the high H_C at the NiO–Co interface. Observation of domain configurations during reversal of Ni(50 nm)–NiFe(10 nm) bilayers grown on (0 0 1)MgO were reported by Nikotenko et al. [53], using a magneto-optical indicator. At the resolution of this method ($\approx$ several μm), they observed that domain nucleation was responsible for magnetization reversal when the field was applied along H_E, but that incoherent reversal occurred in transverse fields. Another interesting observation was that the wall nucleation initiated at film edges with fields antiparallel to H_E, but nucleation occurred at dislocation slip planes and their intersections for applied fields parallel to H_E.

Although T_N is relatively high in NiO, its low K_2 can lead to thermal instability if the grain size is small, since the energy barrier against thermally activated reversal is $\propto K_2V$. Soeya et al. [54] examined H_E of exchange-coupled 40 nm $Ni_{81}Fe_{19}$ films after field-cooling from above T_N, and then cooling from $T \leqslant T_N$ in both 500 Oe DC fields opposite to the initial cooling-field direction or an AC field of 40 Oe perpendicular to the cooling field in the plane of the films. In both cases, H_E decreased monotonically with higher starting temperatures. They interpreted this behavior as indicating the presence of a distribution of different exchange-coupling paths at the interface, each with differing T_Bs. This is certainly a plausible model, which was initially introduced by Tsang and Lee [55], and by Speriosu et al. [56] for FeMn–$Ni_{81}Fe_{19}$. Similar results were reported by Ohshima et al. [57]. They investigated $Ni_{80}Fe_{20}$ films coupled to both NiO and FeMn. They applied fields perpendicular to the direction of H_e in the film plane at temperatures of 323 and 373 K for various times. They examined the phase shift of the unidirectional component of the torque curve after the thermal treatments. The shifts increased and the torque amplitudes decreased linearly with log time, leading them to ascribe this behavior to a thermal fluctuation aftereffect, in the spirit of Néel [9] and Fulcomer and Charap [10,11]. Similar results were reported by van der Heijden et al. [58] for NiO–$Ni_{66}Co_{18}Fe_{16}$ bilayers. They concluded that the AFM grains were not single domains. Thus walls were likely important in these structures. They also noted that the AFM grains could have a small moment due to uncompensated spins, enabling a direct coupling of these grains to the applied field.

A very unique exchange anisotropy situation has been reported for the Fe–FeF_2 system. FeF_2 has a body-centered tetragonal structure with the Fe^{2+} cations located at the cube corners and center [59]. At 78.4 K, AFM ordering puts the Fe^{2+} spins along the *c*-axis, with the cube corner spins antiparallel to those at the body-center position, with an accompanying uniaxial magnetocrystalline anisotropy [60,61]. The remarkable fact is that when FeF_2($\approx$90 nm)–Fe($\approx$13 nm) bilayers grown on (0 0 1)MgO are field-cooled below T_N, the magnitude and sign of H_E depend on the magnitude of the cooling field [62]. Thus, after cooling in positive fields, H_E increases from ~ -200 Oe to $+200$ Oe monotonically with increasing applied cooling fields up to 70 kOe, and the sign of H_E remains constant until $T_B = T_N$ is reached. The authors' model for this behavior is that high fields begin moving AFM interfacial spins into the field direction, and these spins couple antiferromagnetically with the interfacial FM spins. Several other papers by the same group have considered a variety of aspects of this system [63–65]. An important finding was that the exchange-bias effects can be quite large ($\sim$1.1 erg/cm^2), and that the magnitude of the exchange bias field increases with interfacial roughness.

2.2. Exchange couples with metallic AFM films

Since almost all of the current applications of exchange anisotropy for film biasing use metallic

AFMs, it might be expected that reliable modeling of exchange biasing with these systems would be more extensive than for the insulating AFMs. However, although many more investigations have been reported for exchange couples using metallic AFM films than for insulating ones, it seems that there is actually less understanding of the basic phenomena when metallic AFM films are involved. There are several likely reasons for this situation. The crystal structures of metallic AFMs often deviate more strongly from cubic symmetry than do the structures of the insulating AFMs. This makes it more difficult to grow suitable epitaxial films, whether bilayer or multilayer. The spin structures are generally more complex in metallic AFM; i.e. multi-spin sublattices, as well as temperature-dependent spin phases. The T_Ns of the metallic AFMs are usually higher than for insulating AFMs. This means that it is not always possible to field-cool through T_N without risking irreversible structural changes such as grain growth and interdiffusion. Thus, it is not as convenient to work with model systems as with insulating AFM.

Virtually all of the metallic AFM materials investigated for exchange-biasing have been Mn alloys. The seminal paper in this connection was by Hempstead et al. [66], in which it was reported that depositing γ-phase FeMn ($\sim$50% Mn) films onto $Ni_{80}Fe_{20}$ films produced larger loop shifts and higher H_E/H_C ratios than were obtained for couples consisting of either annealed $Ni_{80}Fe_{20}$/Mn or $Ni_{80}Fe_{20}$/α-Fe_2O_3. They noted that although the γ-phase of Mn was not stable at room temperature in the bulk, the γ-phase of FeMn in films was stable, and could be deposited on the $Ni_{80}Fe_{20}$, even without annealing. They suggested a number of ternary additions to further stabilize the γ-phase, and pointed out that bulk binary alloys of Mn with Fe, Ni, Rh, Pt and ternary alloys with Ni and Fe are γ-phases, and exhibit unidirectional properties. They also noted that unidirectional anisotropy was produced in their $Ni_{80}Fe_{20}$/FeMn couples without cooling from above T_N, and that the direction of the exchange bias could be moved into the direction of a field applied at temperatures much lower than T_N. Finally, they stressed the importance of the nature of the FM/AFM interface. These points made by Hempstead et al. have consistently reappeared in the extensive subsequent work on exchange couples with metallic AFMs.

2.2.1. Fe–Mn

AFM Fe–Mn films with various additions are currently in use in most exchange-biased MR read-heads. The AFM γ-phase is FCC, and extends from about 30–55 at% Mn at room temperature [67]; T_N increases from about 425–525 K with increasing Mn concentration in this range. Most investigations use alloys with 50% or more Mn to achieve the higher T_N (and, hence, T_B). The Mn and Fe atoms occupy the lattice sites randomly. The atoms at the (0, 0, 0), $(0, \frac{1}{2}, \frac{1}{2})$, $(\frac{1}{2}, 0, \frac{1}{2})$, and $(\frac{1}{2}, \frac{1}{2}, 0)$ form a tetrahedron, and the spins on these atoms are directed along the four $\langle 1\,1\,1\rangle$ directions towards the center of this tetrahedron [67]. When FCC permalloy ($Ni_{81}Fe_{19}$) is the FM, lower H_C is achieved when the FeMn is deposited on the permalloy than when the deposition order is reversed, and the substrate is not FCC.

The issues of deposition order and of the influence of FeMn thickness were explored by Kung et al. [68], who characterized trilayers of NiFe(60 nm)/FeMn(4–40 nm)/NiFe(30 nm)/Ta(20 nm). The lower and upper interface coupling behavior could be readily distinguished by hysteresis loop measurements. The interfacial unidirectional energy density, $\Delta\sigma$ (erg/cm^2) is commonly defined by

$$H_E = \Delta\sigma / M_{FM} t_{FM},$$

where t_{FM} is the thickness of the FM film. For the lower interface, $\Delta\sigma$ and T_B both increase initially with FeMn thickness, but become constant for FeMn thicknesses beyond 8 and 16 nm, respectively. For the upper interface, $\Delta\sigma$ and T_B both increase initially, but start to decrease for FeMn thicknesses above 12 and 36 nm, respectively. Kung et al. found that the FeMn grain size increased with thickness, and suggest that the initial increase in $\Delta\sigma$ and T_B are due to an average increase in grain size and that the decrease for thick FeMn are due to roughness and the loss of the γ-phase. Although this is a plausible explanation, it is simpler to explain the decrease in $\Delta\sigma$ at the upper interface as reflecting a decreasing density of uncompensated spins with increasing interfacial AFM grain size as the FeMn

thickness increases, as was found for the CoO–$Ni_{81}Fe_{19}$ system [34,35].

Jungblut et al. [69] investigated the influence of interfacial orientation on H_E and H_C in epitaxial $Ni_{80}Fe_{20}/Fe_{50}Mn_{50}$ bilayers. They described the very different spin structures terminating the (0 0 1), (1 1 1), and (1 1 0)$Fe_{50}Mn_{50}$ surfaces, and grew wedge-shaped bilayers in these orientations with varying thicknesses of the FM and AFM layers. They discussed their findings in terms of various models and structural features. The general conclusions were that while H_E and H_C and their ratios depended strongly on interfacial orientation, there was no indication that the compensated or uncompensated nature of an 'ideal' interface played a significant role in determining these properties.

A number of papers have interpreted the temperature dependence of H_E, H_C, and T_N in terms of several interfacial issues, e.g., interfacial magnetic disorder [51], varieties of exchange paths [70], directional distributions of pinning fields due to the polycrystalline interface [71] or interfacial structural features [72,73]. These considerations are evidence of the growing recognition that detailed atomic scale magnetic and structural characterization of the FM–AFM interface is the key to understanding exchange anisotropy phenomena.

2.2.2. Ni–Mn

The search for higher T_B and a more corrosion-resistant AFM has led to the characterization of a number of other Mn-based alloys. The ordered FCT Θ-phase of Ni–Mn extends from $\sim$43 to $\sim$53 at%Mn [74]. The Mn atoms, with moments $\approx$3.8 μ_B, and the Ni atoms, with virtually no moment ($< 0.2\ \mu_B$), are alternately placed on (0 0 2) planes [74,75]. The nearest-neighbor Mn atoms are coupled AFM, with the next-nearest-neighbors FM. At temperatures $> \sim$1050 K, the Θ-phase transforms to a disordered BCC phase, and the magnetic order disappears [74]. Lin et al. [76] compared H_E and H_C of $Ni_{50}Mn_{50}$ and $Fe_{46}Mn_{54}$ bilayers with $Ni_{81}Fe_{19}$. After annealing at 240 and 255°C for 240 and 255 h, respectively, the bilayers with $Ni_{50}Mn_{50}$ had $\Delta\sigma$ values of 0.27 erg/cm^2, three times that of the $Fe_{46}Mn_{54}$ biased films. T_B was $>$ 400°C for the $Fe_{46}Mn_{54}$ film, as compared to $\sim$150°C for the $Fe_{46}Mn_{54}$ biased film. Corrosion resistance was also superior for the $Ni_{50}Mn_{50}/Ni_{81}Fe_{19}$ bilayer. However, the annealing to produce the AFM FCT phase increased H_C to 47 Oe, as compared to 5 Oe for the $Fe_{46}Mn_{54}/Ni_{81}Fe_{19}$ bilayer.

2.2.3. Ir–Mn

In the disordered FCC (γ) phase from $\sim$10 to $\sim$30 at% Mn, T_N increases from $\sim$600 to $\sim$750 K [77]. The average spins on each (0 0 2) plane are aligned parallel along the *c*-axis with alternating signs on neighboring (0 0 2) planes [77,78]. The average moments per atom are $\sim$2.5 μ_B up to $\sim$20 at% Mn, and drop to 0.8 μ_B at $\sim$25.6 at% Mn [58]. Fuke et al. [79]. characterized spin valves in which $Ir_{20}Mn_{80}$ films were used to bias $Co_{90}Fe_{10}$ films. H_E varied inversely with the $Co_{90}Fe_{10}$ thickness, and $\Delta\sigma$ was 0.19 erg/cm^2 at room temperature for the as-deposited couples, and decreased to about 0.16 erg/cm^2 after annealing at 280°C for 5 min in an applied field. $\Delta\sigma$ decreased monotonically with temperature, and T_B was $\sim$265°C before and after the anneals. H_C for the as-deposited films was $\approx$100 Oe.

2.2.4. Pt–Mn

Chemically ordered Pt–Mn alloys are AFM with T_N ranging from 485 K for 66 at% Mn to a maximum value of 975 K at the equiatomic composition, decreasing to 815 K at 41 at% Mn [80,81]. Utilizing these high T_N values requires achieving the ordered structure in films. Farrow et al. [82] prepared a number of polycrystalline an epitaxial couples of $Mn_xPt_{(1-x)}$ with permalloy using a variety of substrates and underlayers to encourage growth of an ordered structure. Their X-ray diffraction data were generally consistent with an ordered structure for films grown at 200°C. The best results were obtained on an MgO(0 0 1) substrate with a 18.6 nm $Mn_{56}Pt_{44}$ film. $\Delta\sigma$ was 0.032 erg/cm^2 at room temperature, and H_C was 19 Oe for the 10.9 nm permalloy film. $\Delta\sigma$ decreased monotonically from 77 K, and extrapolated values from MR data suggested a $T_B > 500$ K. However, heating the film to 180°C for the MR measurements decreased $\Delta\sigma$, possibly due to interdiffusion.

2.2.5. Rh–Mn

Ordered Mn_3Rh has a triangular spin arrangement below its T_N of 850 K. Velosa et al. [83] have investigated spin valves with $Mn_{78}Rh_{22}$ films biasing $Co_{90}Fe_{10}$. $\Delta\sigma$ was ≈ 0.19 erg/cm^2, and T_B was $\sim 250^\circ$C.

2.2.6. Other Mn-based AFM films

Several ternary AFM Mn-based alloys have been examined. These include Pd–Pt–Mn [84,85] and Cr–Mn–Pt [86]. A particularly comprehensive comparison of the properties of FeMnRh, IrMn, RhMn, PdPtMn, NiMn, and CrPtMn has been reported by Lederman [87].

3. Models and theories

3.1. Ideal interfaces

The first simple model of exchange anisotropy examined the exchange coupling across an ideal interface as shown in Fig. 2. The FM and AFM layers are both single crystalline and epitaxial across an atomically smooth FM/AFM interface. AFM materials have no net moment. The AFM monoxides are composed of atomic planes of ferromagnetically oriented spins with anti-parallel alignment between adjacent planes. In Fig. 2, the interfacial AFM spin plane is fully uncompensated. During the reversal of the FM magnetization in this ideal model, the spins of the FM layer rotate coherently, while the spins of the AFM layer remain fixed. The energy cost is equal to the interfacial exchange energy. The phenomenological formula of the exchange field is

$$H_E = \frac{\Delta\sigma}{M_{FM}t_{FM}} = \frac{2J_{ex}\boldsymbol{S}_{FM}\cdot\boldsymbol{S}_{AFM}}{a^2 M_{FM}t_{FM}}, \quad (1)$$

where $\Delta\sigma$ is the interfacial exchange energy density, J_{ex} is the exchange parameter, $\boldsymbol{S}_{FM}$ and $\boldsymbol{S}_{AFM}$ are the spins of the interfacial atoms, and a is the cubic lattice parameter. In the $Ni_xCo_{(1-x)}O$ system, an atomically smooth $\langle 1\,1\,1\rangle$ oriented single crystal should result in a fully uncompensated interfacial spin plane as depicted in the ideal model. Therefore, one may expect a FM layer coupled to a $\langle 1\,1\,1\rangle$ oriented $Ni_xCo_{(1-x)}O$ single crystal to exhibit an exchange field magnitude as predicted by Eq. (1). Using reasonable parameters, one obtains values of $\Delta\sigma \sim 10$ erg/cm^2. However, as discussed above, the observed exchange fields for single- and polycrystalline AFM films of all types are two-to-three orders smaller. Clearly, this simple ideal model does not realistically represent the FM/AFM interfacial environment.

Phenomena such as interfacial contamination or roughness have been invoked to account for the reduction of interfacial coupling strength. Roughness in the form of interfacial atomic steps could produce neighboring antiparallel spins and thereby reduce the number of interfacial uncompensated spins. Other experimental studies have raised other questions. If only the $\langle 1\,1\,1\rangle$ spin planes are fully uncompensated, one may expect that single crystals of any other crystalline orientation would exhibit small or no exchange field due to a compensated interfacial spin plane. Polycrystalline films are composed of subunits or grains which possess a distribution of orientations, predominantly not $\langle 1\,1\,1\rangle$. Yet FM films coupled to polycrystalline AFM films often have higher exchange fields than FM films coupled to single crystal $\langle 1\,1\,1\rangle$ films. Perhaps the uncompensated spins originate from the disordered regions within the grain boundaries. These are simply qualitative explanations and do not provide for quantitative analysis and comparison with experimental observations. A model of the exchange bias mechanism must resolve the following discrepancies and questions:

1. What structural and magnetic parameters are responsible for the drastic reduction of the interfacial exchange energy density from the ideal case?
2. What are the origin and role of the interfacial uncompensated AFM spins?
3. How is the magnitude of the exchange field dependent upon the AFM grain structure?
4. What determines the temperature dependence of the exchange field?
5. What are the roles of interfacial exchange J_{ex} and AFM magnetocrystalline anisotropy K_{AFM} in unidirectional anisotropy?

In the past decade, a number of models and theories have been proposed to provide qualitative and quantitative descriptions of the exchange biasing mechanism.

3.2. Interfacial AFM domain wall

To explain the discrepancy between the exchange field value predicted by simple theory and experimental observations, Mauri et al. [88] proposed a mechanism that would effectively lower the interfacial energy cost of reversing the FM layer without removing the condition of strong interfacial FM/AFM coupling. They proposed the formation of a planar domain wall at the interface with the reversal of the FM orientation. The domain wall could be either in the AFM or FM, wherever the energy is lower. They examined the case where the domain wall forms in the AFM side of the interface. With the magnetization reversal of the FM layer, the increase in interfacial exchange energy would be equal to the energy per unit area of an AFM domain wall $4\sqrt{A_{AF}K_{AF}}$, where A_{AF} and K_{AF} are the exchange stiffness ($\sim J_{AF}/a$) where J_{AF} is the AFM exchange integral parameter, and a is the AFM lattice parameter) and AFM magnetocrystalline anisotropy, respectively. Thus, the modified expression for the exchange field would be

$$H_E = \frac{2\sqrt{A_{AF}K_{AF}}}{M_{FM}t_{FM}}. \tag{2}$$

By spreading the exchange energy over a domain wall width $\sim\pi\sqrt{A_{AF}K_{AF}}$ instead of a single atomically wide interface, the interfacial exchange energy is reduced by a factor of $\pi\sqrt{A_{AF}K_{AF}}/a$, ≈ 100, which would provide the correct reduction to be consistent with the observed values. Smith and Cain [89] fitted the magnetization curves of permalloy/TbCo bilayer films using a similar model with strong interfacial coupling.

Mauri et al. assume that: (i) an AFM domain can form at the interface; (ii) the AFM layer is infinitely thick (no restrictions for the AFM domain wall formation due to thickness); and (iii) the spins within the FM rotate coherently (for the case of the FM layer thickness less than the thickness of a domain wall). They use a Hamiltonian that accounts for AFM domain wall energy, interfacial exchange energy, FM anisotropy energy, and a magnetostatic energy term. Magnetization curves were calculated by minimizing the energy with two free parameters: α (which represents the angular displacement of the interfacial AFM spins from the AFM Néel axis), and β (the angular displacement of the coherent FM spins from the easy-axis). The AFM Néel axis and the FM easy-axis are parallel. A numerical calculation over a range of interfacial exchange energies yields the following two limiting cases:

Strong interfacial coupling

$$\Rightarrow H_{ex} = -2\left(\frac{\sqrt{A_{AF}K_{AF}}}{M_S t_{FM}}\right), \tag{3}$$

Weak interfacial coupling

$$\Rightarrow H_{ex} = -\left(\frac{J_{ex}}{M_S t_{FM}}\right), \tag{4}$$

where J_{ex} is the effective interfacial coupling energy, and t_{FM} and M_S are the thickness and saturation magnetization of the FM, respectively. In the case of strong interfacial exchange coupling ($J_{ex} \gg \sqrt{A_{AF}K_{AF}}$), H_{ex} saturates at energies far less than the fully uncompensated interfacial exchange coupling case due to the formation of an interfacial AFM domain wall. In the case of weak interfacial exchange coupling ($J_{ex} \ll \sqrt{A_{AF}K_{AF}}$), H_{ex} is limited by the strength of the interfacial exchange coupling J_{ex}. The model offers no insight as to the origins of the reduced interfacial coupling, nor does it address the origin of the coupling with compensated spin planes. This model highlights the formation of an AFM planar domain wall in the limit of strong interfacial exchange; however, most experimental studies indicate the presence of weak interfacial exchange. Thus, this model does not shed light on the mechanism responsible for the reduced interfacial exchange coupling energy density.

3.3. Random field model

Malozemoff rejects the assumption of an atomically perfect uncompensated boundary exchange.

He proposed a random-field model [90–92] in which an interfacial AFM moment imbalance originates from features such as roughness and structural defects. Thus, the interfacial inhomogeneities create localized sites of unidirectional interfacial energy by virtue of the coupling of the net uncompensated moments with FM spins. For interfacial roughness that is random on the atomic scale, the local unidirectional interface energy σ_l is also random, i.e.

$$\sigma_l = \pm z\frac{J}{a^2}, \tag{5}$$

where J is the interfacial exchange parameter, a is cubic lattice parameter, z is a number of order unity. Random-field theory argues that a net average non-zero interfacial energy will exist, particularly when the average is taken over a small number of sites. Statistically, the average σ in an area of L^2 will decrease as $\sigma \approx (\sigma_l/\sqrt{N})$ where $N = (L^2/a^2)$ is the number of sites projected onto the interface plane. Given the random field and assuming a single domain FM film, the AFM film will divide into domain-like regions to minimize the net random unidirectional anisotropy. Unlike Mauri et al.'s model, the AFM domain walls in Malezemoff's model are normal to the interface. Initiation of the AFM domain pattern occurs as the FM/AFM bilayer is cooled through T_N.

Although expansion of the domain size L would lower the random field energy, in-plane uniaxial anisotropy energy K in the AFM layer will limit the domain size. Anisotropy energy confines the domain wall width to $\pi\sqrt{A/K}$ ($<L$), and creates an additional surface energy term of the domain wall $4\sqrt{AK}$ (surface tension in bubble domain). The balance between exchange and anisotropy energy is attained when $L \approx \pi\sqrt{A/K}$. Therefore, the average interfacial exchange energy density $\Delta\sigma$ becomes

$$\Delta\sigma = \frac{4zJ}{\pi aL}. \tag{6}$$

Accordingly, the exchange field due to the interfacial random-field energy density is

$$H_E = \frac{\Delta\sigma}{2M_{FM}t_{FM}} = \frac{2z\sqrt{AK}}{\pi^2 M_{FM}t_{FM}} \tag{7}$$

using the equilibrium domain size expression for L. This equation is very similar to the strong interfacial exchange case (Eq. (3)) of Mauri et al.'s planar interfacial AFM domain wall model. Thus, quantitatively, the random-field model also accounts for the 10^{-2} reduction of the exchange field from the ideal interface model case.

In addition to the reduction of the interfacial exchange energy, Malozemoff's model attempts to explain the following magnetic behavior associated with exchange anisotropy: (1) approximately linear falloff $(1 - T/T_{crit})$ of exchange field, (2) the magnetic training effect [9] (as the unwinding of domain state and the annihilation of domains with field cycling), and (3) critical AFM thicknesses for exhibiting an exchange field. Malozemoff has tried to account for a number of the key experimental observations associated with exchange biasing. Malozemoff's model is specifically formulated for single crystal AFM systems and does not clearly propose how the model can be extended to polycrystalline systems. The argument of a statistical basis for the density of uncompensated spins is intriguing but not explicitly convincing.

3.4. '*Spin-flop*' *perpendicular interfacial coupling*

The 'spin-flop' model introduced by Koon [93] presents a novel solution to a particular issue of exchange biasing. On the basis of his micromagnetic numerical calculations, Koon proposed the existence and stability of unidirectional anisotropy in thin films with a fully *compensated* AFM interface. His calculations indicate the stability of interfacial exchange coupling with a perpendicular orientation between the FM and AFM axes directions. He refers to the perpendicular interfacial coupling as 'spin-flop' coupling. One limitation of Koon's model is that he examines a very specific system. To observe perpendicular interfacial coupling, his model specifies the structure and orientation of the AFM layer, and the relative orientation between the AFM and FM layer. His results are suggestive but difficult to apply to other systems. The model utilizes a single-crystal body centered tetragonal (BCT) AFM structure as shown in Fig. 5a. The BCT structure can be oriented to have a fully uncompensated interfacial spin plane (1 0 0)

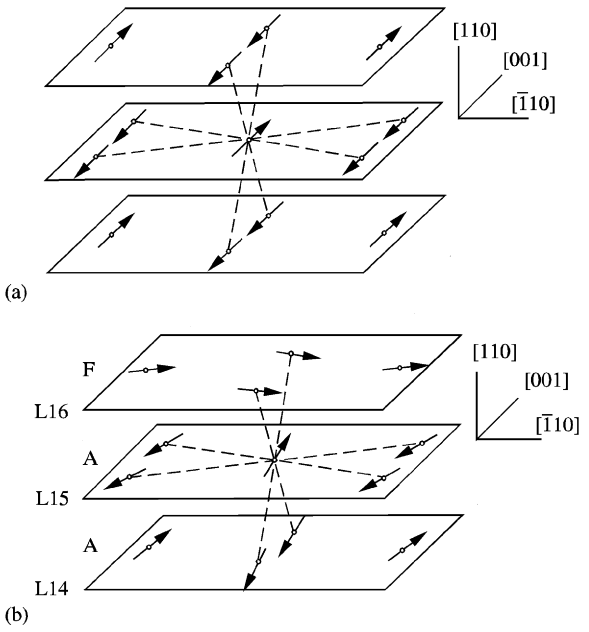

Fig. 5. (a) Magnetic structure of a $\langle 1\,1\,0\rangle$ oriented AFM body centered tetragonal crystal. The exchange bonds are represented by the dashed lines. (b) Lowest energy spin configuration near the interface plane. The interfacial AFM plane (L15) is fully compensated, and the interfacial FM plane (F16) is oriented perpendicular (90° coupling). The angles are approximately to scale. From Ref. [93].

or a fully compensated interfacial spin plane (1 1 0) (shown in Fig. 5a). He included uniaxial anisotropy in the AFM crystal along the (0 0 1) axis, and the FM layer was modeled with no intrinsic anisotropy.

Koon applied his model to two different cases of the AFM interfacial spin plane: (1) a fully compensated interface and (2) a fully uncompensated interface. For both cases, he calculated the interfacial energy density as a function of the angle between the FM spins and the Néel axis of the AFM spins. The fully uncompensated interface gives the expected results of collinear coupling, a minimum at $\theta = 0°$. However, the fully compensated interface gives the surprising result of an energy minimum at $\theta = 90°$ indicating perpendicular interfacial coupling between the FM and AFM spins. Fig. 5b shows the spins configuration near the interface plane, illustrating the perpendicular orientation of the FM and AFM axes.

In his published work, Koon hypothesizes that roughness would reduce frustration and reduce biasing from the fully compensated case. However, his unpublished work suggested that the introduction of roughness into his model resulted in the transition from perpendicular to collinear coupling. The transition may be attributed to the increasing density of uncompensated interfacial AFM spins. The issue of perpendicular interfacial coupling in FM/AFM bilayers may be more relevant in smooth single crystals than in polycrystalline films.

The recent work by Schulthess and Butler [94] yielded findings contrary to Koon's calculations. They adopted Koon's spin configurations but implemented a classical micromagnetic approach using the Landau–Lifshitz equation of motion with the Gilbert–Kelley form for a damping term. Their work yielded the interfacial spin-flopped state similar to Koon's, but had contrary conclusions with respect to exchange biasing. Their calculations indicated enhanced uniaxial anisotropy or enhanced coercivity, but not a shifted magnetization curve. The difference is attributed to an additional degree of freedom which creates a lower energy barrier. However, the introduction of interfacial defects shifts the energy minima of the two spin-flopped states. The asymmetry in the energy minima results in the observation of an exchange bias. They noted that the unidirectional shift results from the coupling of the FM to the uncompensated defects on the AFM interface, and spin-flop coupling is not a requirement for observing exchange bias.

3.5. Uncompensated interfacial AFM spins

Meiklejohn and Bean originally suggested that unidirectional exchange anisotropy was a consequence of the presence of interfacial uncompensated AFM spins. The experimental correlation between the interfacial uncompensated CoO spins and the exchange field in polycrystalline CoO/permalloy bilayer films was only recently demonstrated by Takano et al. [34,35]. They measured the uncompensated spins on the surfaces of antiferromagnetic CoO films as a thermoremanent magnetization (TRM) after field-cooling a series of CoO/MgO multilayers from $T > T_N$. The temperature dependence of the TRM was similar to the

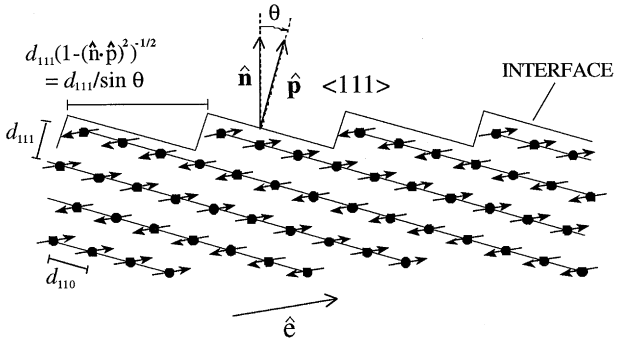

Fig. 6. Schematic of interface cross section. Film normal is $\hat{n}$, $\hat{p}$ is the normal to the parallel spin plane (1 1 1) of the AFM, and $\hat{e}$ is the AFM spin axis (in this case $N_{\text{rows}} = 4$). From Refs. [34,35].

temperature dependence of the sublattice magnetization for bulk CoO materials as determined by neutron diffraction [95]. These measurements showed that the spins responsible for this uncompensated AFM moment are interfacial and constitute $\sim 1\%$ of the spins in a monatomic layer of CoO. This low density is consistent with the low exchange fields observed compared to the values predicted by the ideal interface model (see Eq. (1)). The uncompensated AFM TRM also has the same temperature dependence as the exchange field of $Ni_{81}Fe_{19}$/CoO bilayers after field-cooling. Thus, the uncompensated interfacial AFM spins appear to be the spins responsible for unidirectional anisotropy. Takano et al. determined that a linear relationship exists between the strength of the exchange field and the inverse of the CoO crystallite diameter, i.e., $H_E \propto L^{-1}$, where L is the grain diameter. This suggests a structural origin for the density of uncompensated spins.

The magnitude and the temperature dependence of the exchange field in FM/CoO bilayers correlate with the density of uncompensated interfacial CoO spins, but what are the structural origins of the uncompensated spins in polycrystalline AFM films? To answer this question, Takano et al. calculated the density of interfacial uncompensated spins as a function of grain size, orientation, and interfacial roughness of polycrystalline AFM films. Each CoO crystallite was assumed to be a single AFM domain. Fig. 6 is a view of the interfacial cross section of an AFM crystal showing that the orientation of the AFM determines the periodicity with which the (1 1 1) ferromagnetic spin planes intercept the interface. Fig. 7a is a plan view of the same AFM crystal. The crystalline orientation is reflected in the periodic alternating pattern of four rows. In Fig. 7a, an elliptical sampling region simulating a grain with a major axis length L has been superimposed onto the spin map. The number of uncompensated spins $\langle \Delta N \rangle$ for a model crystallite was computed by simply adding the total number of spins in each direction contained within the boundaries of the model grain. The fundamental origin of uncompensated AFM moment is scale. Although the large spin map may represent compensated spin regions, one observes small densities of uncompensated spins when sampling small areas within the spin map. Thus, one will observe an exchange bias with polycrystalline AFM films regardless of whether the preferred orientation suggests that the interfacial plane is completely compensated. Interfacial roughness was incorporated onto the spin maps by superimposing elliptical 'islands' of monatomic thickness on the spin map. The effect of adding one atomic layer is to reverse the direction of the spin at each site covered by the island, since successive layers of CoO spins have opposite direction (see Fig. 7b). Takano et al. created a series of large spin maps several times larger than the model grain sizes to be sampled. Fig. 8 is an example of one of the large spin maps containing the topographical roughness features. Statistical averages were obtained from sampling 10^6 model crystallites by varying the position, orientation of the major axis, and aspect ratio of the

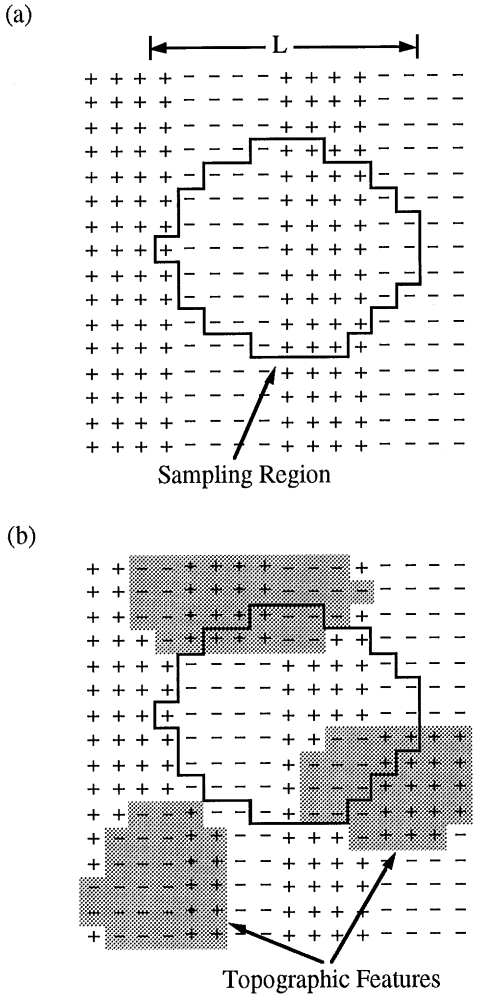

Fig. 7. (a) Topographical representation of the interfacial plane. Periodic pattern of $N_{rows} = 4$ (as in Fig. 6) with a sample region representing a model crystallite. (b) Topographical representation of the interfacial plane. Elliptical 'islands' of monatomic layer thickness were superimposed on the spin map to simulate roughness. Note that adding one atomic layer reverses the direction of the underlying spin. From Refs. [34,35].

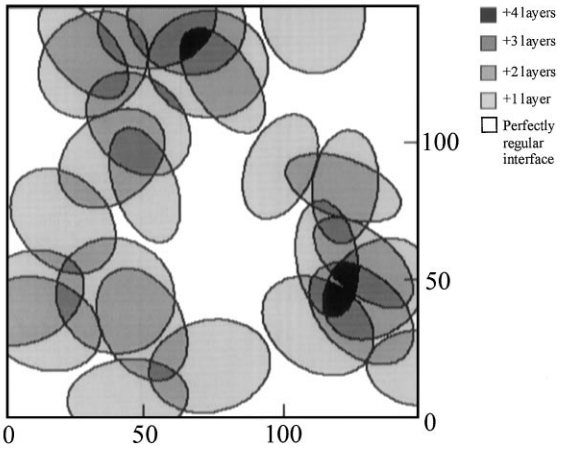

Fig. 8. Topographical map containing overlapping 'islands'. The islands have a feature diameter of 20 lattice parameters and coverage equal to the total area of the map. The legend correlates the different shades of gray with the height of interfacial elevation above the base spin pattern [see Fig. 7a]. From Refs. [34,35].

model crystallite. Two primary results of these calculations are: (1) a perfectly regular interface without any roughness features results in $\langle \Delta N \rangle \propto L^{0.5}$; (2) the addition of roughness results in $\langle \Delta N \rangle \propto L^{0.90 \sim 1.04}$. Since the exchange field is proportional to $\langle \Delta N \rangle / L^2$, the rough case gives $H_E \propto L^{-1}$, in agreement with the experimental results. Using realistic and experimental values, the observed exchange field for a 10 nm CoO biasing film was consistent with interfacial roughness of only a few 'extra' atomic steps across the face of each crystallite. Thus, the model correctly predicts the inverse dependence of the uncompensated spins on grain size and the correct magnitude of H_E. The model indicates that the origins of the uncompensated AFM interfacial moment are (i) the dimensions of the AFM grain boundaries and (ii) the presence of interfacial roughness features.

The combination of the experimental results and the model is very comprehensive in explaining many of the issues and questions concerning the mechanism behind exchange biasing. The origin of the exchange biasing mechanism is indeed the uncompensated interfacial AFM spins. The magnitude and temperature dependence of the exchange field can be explained from the measurements of the magnetic properties of the uncompensated AFM spins. The model has demonstrated the structural origins of the uncompensated AFM moment in polycrystalline films. Neither the experimental results nor the model shed any light on the type of interfacial coupling, i.e. collinear

versus perpendicular coupling. CoO has very high magnetocrystalline anisotropy which results in a direct correlation of the uncompensated moment and the exchange field. Other AFM materials with lower anisotropy, such as NiO, do not exhibit this correlation due to complications not included in this model. Future models can attempt to model the complex behavior for AFM systems with low bulk or surface anisotropy.

4. Concluding comments

Using the rather demanding criterion of major technological application, it is clear that substantial progress has been made in elucidating some qualitative details concerning the phenomenon of exchange anisotropy. However, in common with most other magnetic phenomena in which surface and/or interfacial properties are important, there exists no basic, generally applicable, predictive theory/model. The reason for this state of our knowledge in exchange anisotropy is that the essential behavior depends critically on the atomic-level chemical and spin structure at a buried interface, and the tools to uncover this type of information — e.g., atomic level chemical and spin-selective photo-emission, Mössbauer spectroscopy, neutron diffraction, chemically resolved TEM imaging — are just beginning to be applied to this problem. Even if this atomic level information becomes available, it is likely that the interfacial chemical and spin structures are too complex for ab initio modeling.

A more promising view is that considerable progress has been achieved. The interfacial complexity has been recognized as the major factor and is being investigated. The hitherto puzzling low $\Delta\sigma$ has been convincingly explained in at least one case as arising from the low density of the uncompensated interfacial AFM spins. Hopefully, this will turn out to be a general conclusion. This is just one of several explanations of exchange anisotropy phenomenon proposed by Meiklejohn and Bean, and by Néel, that have been made more quantitative or have been reinforced by experiment. Other examples are the significance of the AFM magnetocrystalline anisotropy as compared to the interfacial exchange interaction, and the various viscosity effects. This significant progress, the increasing availability of methods for examining buried interfaces, and the technological demand for higher H_E and T_B, are probably reason enough to be optimistic about achieving a continually better understanding of this fascinating phenomenon.

Acknowledgements

The preparation of this paper was partially supported by the NSF.

References

[1] W.H. Meiklejohn, C.P. Bean, Phys. Rev. 102 (1956) 1413.
[2] W.H. Meiklejohn, C.P. Bean Phys. Rev. 105 (1957) 904.
[3] W.H. Meiklejohn, J. Appl. Phys. Suppl. 33 (1962) 1328.
[4] I.S. Jacobs, C.P. Bean, in: G.T. Rado, H. Suhl (Eds.), Magnetism, Vol. III, Academic Press, New York, 1963, pp. 272–350.
[5] A. Yelon, in: M.H. Francombe, R.W. Hoffman (Eds.), Physics of Thin Films, Vol. 6, Academic Press, New York, 1971, pp. 213–223.
[6] A.E. Berkowitz, J.H. Greiner, J. Appl. Phys. 36 (1965) 3330.
[7] J.S. Kouvel, J. Phys. Chem. Solids 24 (1963) 795.
[8] T. Satoh, R.B. Goldfarb, C.E. Patton, J. Appl. Phys. 49 (1978) 3439.
[9] L. Néel, Ann. Phys. 2 (1967) 61.
[10] S.H. Charap, E. Fulcomer, Phys. Stat. Sol. (a) 11 (1972) 559.
[11] E. Fulcomer, S.H. Charap, J. Appl. Phys. 43 (1972) 4184.
[12] O. Bostanjoglo, P. Kreisel, Phys. Stat. Sol. (a) 7 (1971) 173.
[13] O. Bostanjogglo, W. Giese, Int. J. Magn. 3 (1972) 135.
[14] H. Neal Bertram, Theory of Magnetic Recording, Cambridge University Press, Cambridge, 1994.
[15] P.D. Battle, A.K. Cheetham, G.A. Gehring, J. Appl. Phys. 50 (1979) 7578.
[16] H.P.J. Wijn (Ed.), Landolt-Börnstein, Numerical Data and Functional Relationships in Science and Technology, Vol. III/27g, Springerl, Berlin, 1991, p. 30.
[17] W.L. Roth, J. Appl. Phys. 31 (1960) 200.
[18] W.L. Roth, G.A. Slack, J. Appl. Phys. Suppl. 31 (1960) 352S.
[19] G.A. Slack, J. Appl. Phys. 31 (1960) 1571.
[20] J. Kanamori, Prog. Theor. Phys. 17 (1957) 197.
[21] A.J. Sievers III, M. Tinkham, Phys. Rev. 129 (1963) 1566.
[22] H. Kondoh, J. Phys. Soc. Japan 15 (1960) 1970.
[23] M.T. Hutchings, E.J. Samuelson, Phys. Rev. B 6 (1972) 3447.
[24] A.J. Sievers III, M. Tinkham, Phys. Rev. 129 (1963) 1566.
[25] J.I. Kaplan, J. Chem. Phys. 22 (1954) 1709.

[26] W.L. Roth, G.A. Slack, J. Appl. Phys. Suppl. 31 (1960) 352S.
[27] E. Uchida, N. Fukuoka, H. Kondoh, T. Takeda, Y. Nakazumi, T. Nagamiyama, J. Phys. Soc. Japan 23 (1969) 1197.
[28] H.W. White, J.W. Battles, G.E. Everett, Solid State Commun. 8 (1970) 313.
[29] K. Kurosawa, M. Miura, S. Saito, J. Phys. C 13 (1980) 1521.
[30] T. Yamada, J. Phys. Chem. Soc. Japan 21 (1966) 650–664.
[31] M.J. Carey, A.E. Berkowitz, Appl. Phys. Lett. 60 (1992) 3060.
[32] M.J. Carey, A.E. Berkowitz, J. Appl. Phys. 73 (1993) 6892.
[33] J.A. Borchers, M.J. Carey, R.W. Erwin, C.F. Majkzak, A.E. Berkowitz, Phys. Rev. Lett. 70 (1993) 1878.
[34] Kentaro Takano, R.H. Kodama, A.E. Berkowitz, W. Cao, G. Thomas, Phys. Rev. Lett. 79 (1997) 1130.
[35] Kentaro Takano, R.H. Kodama, A.E. Berkowitz, W. Cao, G. Thomas, J. Appl. Phys. 83 (1998) 6888.
[36] Kentaro Takano, Ph. D. Thesis, Physics Department, University of California at San Diego, 1998.
[37] D. Martien, K. Takano, A.E. Berkowitz, D.J. Smith, Appl. Phys. Lett. 74 (1999) 1314.
[38] T.J. Moran, J.M. Gallego, I.K. Schuller, J. Appl. Phys. 78 (1995) 1887.
[39] R. Spagna, M.B. Maple, R.E. Sager, J. Appl. Phys. 79 (1996) 4926.
[40] E.N. Abarra, K. Takano, F. Hellman, A.E. Berkowitz, Phys. Rev. Lett. 77 (1996) 3451.
[41] T. Terashima, Y. Bando, Thin Solid Films 152 (1987) 455.
[42] P.J. van der Zaag, R.M. Wolf, A.R. Ball, C. Bordel, L.F. Feiner, R. Jungblut, J. Magn. Magn. Mater. 148 (1995) 346.
[43] P.J. van der Zaag, A.R. Ball, L.F. Feiner, R.M. Wolf, J. Appl. Phys. 79 (1996) 5103.
[44] Y. Ijiri, J.A. Borchers, R.W. Irwin, S.-H. Lee, P.J. van der Zaag, R.M. Wolf, Phys. Rev. Lett. 80 (1998) 608.
[45] Y. Ijiri, J.A. Borchers, R.W. Irwin, S.-H. Lee, P.J. van der Zaag, R.M. Wolf, J. Appl. Phys. 83 (1998) 6882.
[46] C.A. Kleint, M.K. Krause, R. Höhne, T. Walter, H.C. Sammelhack, M. Lorenz, P. Esquinazi, J. Appl. Phys. 84 (1998) 5097.
[47] S.- S Lee, D.-G. Hwang, C.M. Park, K.A. Lee, J.R. Rhee, J. Appl. Phys. 81 (1997) 5298.
[48] D.-H. Han, J.-G. Zhu, J.H. Judy, J. Appl. Phys. 81 (1997) 4996.
[49] R.P. Michel, A. Chaiken, C.T. Wang, L.E. Johnson, Phys. Rev. B 58 (1998) 8566.
[50] W. Stoecklein, S.S.P. Parkin, J.C. Scott, Phys. Rev. B 38 (1988) 6847.
[51] C. Schlenker, S.S.P. Parkin, J.C. Scott, K. Howard, J. Magn. Magn. Mater. 54–57 (1986) 801.
[52] H.D. Chopra, B.J. Hockey, P.J. Chen, R.D. McMichael, W.J. Egelhoff Jr., J. Appl. Phys. 81 (1997) 4017.
[53] V.I. Nikotenko, V.S. Gornakov, L.M. Dedukh, Yu.P. Kabanov, A.F. Khapikov, A.J. Shapiro, R.D. Shull, A. Chaiken, R.P. Michel, Phys. Rev. B 57 (1998) R8111.
[54] S. Soeya, M. Fuyama, S. Tadokoro, T. Imagawa, J. Appl. Phys. 79 (1996) 1604.
[55] C. Tsang, K. Lee, J. Appl. Phys. 53 (1982) 2605.
[56] V.S. Speriosu, S.S.P. Parkin, C.H. Wilts, IEEE Trans. Magn. 23 (1987) 2999.
[57] N. Oshima, M. Nakada, Y. Tskamoto, IEEE Trans. Magn. 34 (1998) 1429.
[58] P.A.A. van der Heijden, T.F.M.M. Maas, W.J.M. de Jonge, J.C.S. Kools, F. Roozeboom, P.J. van der Zaag, Appl. Phys. Lett. 72 (1998) 492.
[59] J.W. Stout, S.A. Reed, J. Am. Chem. Soc. 76 (1954) 5279.
[60] R.A. Erickson, Phys. Rev. 90 (1953) 779.
[61] D.P. Belanger, P. Nordblad, A.R. King, V. Jaccarino, J. Magn. Magn. Mater. 31–34 (1983) 1095.
[62] J. Nogués, D. Lederman, T.J. Moran, Ivan K. Schuller, Phys. Rev. Lett. 76 (1996) 4624.
[63] J. Nogués, D. Lederman, T.J. Moran, Ivan K. Schuller, K.V. Rao, Appl. Phys. Lett. 68 (1996) 3186.
[64] D. Lederman, J. Nogués, Ivan K. Schuller, Phys. Rev. B 56 (1997) 2332.
[65] J. Moran, J. Nogués, D. Lederman, Ivan K. Schuller, Appl. Phys. Lett. 72 (1998) 617.
[66] R.D. Hempstead, S. Krongelb, D.A. Thompson, IEEE Trans. Magn. 14 (1978) 521.
[67] H. Umbayashi, Y. Ishikawa, J. Phys. Soc. Japan 21 (1966) 1281.
[68] K.T.-Y. Kung, L.K. Louie, G.L. Gorman, J. Appl. Phys. 69 (1991) 5634.
[69] R. Jungblut, R. Coehoorn, M.T. Johnson, J. aan de Stegge, A. Reinders, J. Appl. Phys. 75 (1994) 6659.
[70] C. Tsang, K. Lee, J. Appl. Phys. 53 (1982) 2605.
[71] H. Fujiwara, K. Nishioka, C. Hou, M.R. Parker, S. Gangopadhyay, R. Metzger, J. Appl. Phys. 79 (1996) 6286.
[72] C. Hwang, T. Nguyen, Mat. Res. Soc. Symp. Proc. 232 (1991) 211.
[73] B.Y. Wong, C. Mitsumata, S. Prakash, D.E. Laughlin, T. Kobayashi, J. Appl. Phys. 79 (1996) 7896.
[74] E. Krén, E. Nagy, I. Nagy, L. Pál, P. Szabó, J. Phys. Chem. Solids 29 (1968) 101.
[75] J.S. Kasper, J.S. Kouvel, J. Phys. Chem. Solids 11 (1959) 231.
[76] T. Lin, D. Mauri, N. Staud, C. Hwang, J.K. Howard, G. Gorman, Appl. Phys. Lett. 65 (1994) 1183.
[77] T. Yamaoka, M. Mekata, H. Takaki, J. Phys. Soc. Japan 31 (1971) 301.
[78] T. Yamaoka, M. Mekata, H. Takaki, J. Phys. Soc. Japan 36 (1974) 438.
[79] H.N. Fuke, K. Saito, Y. Kamiguchi, H. Iwasaki, M. Sahashi, J. Appl. Phys. 81 (1997) 4004.
[80] E. Krén, G. Kadar, L. Pál, J. Sólyom, P. Szabó, T. Tarnóczi, Phys. Rev. 171 (1968) 574.
[81] J.A. Ricodeau, J. Phys. F 4 (1974) 1285.
[82] R.F.C. Farrow, R.F. Marks, S. Gider, A.C. Marley, S.S.P. Parkin, J. Appl. Phys. 81 (1997) 4986.
[83] A. Velosa, P.P. Freitas, N.J. Oliveira, J. Fernandes, M. Ferreira, IEEE Trans. Magn. 34 (1998) 2343.

[84] H. Kishi, Y. Kitade, Y. Miyake, A. Tanaka, K. Kobayashi, IEEE Trans. Magn. 32 (1996) 3380.
[85] A. Tanaka, Y. Shimizu, H. Kishi, K. Nagasaka, C. Hou, H. Fujiwara, Mater. Res. Soc. Symp. Proc. 517 (1998) 25.
[86] H. Hoshiya, S. Soeya, Y. Hamakawa, R. Nakatani, M. Fuyama, F. Fukui, Y. Sugita, IEEE Trans. Magn. 33 (1997) 2878.
[87] M. Lederman, IEEE Trans. Magn. 35 (1999) 794.
[88] D. Mauri, H.C. Siegmann, P.S. Bagus, E. Kay, J. Appl. Phys. 62 (1987) 3047.
[89] N. Smith, W.C. Cain, J. Appl. Phys. 69 (1991) 2471.
[90] A.P. Malozemoff, Phys. Rev. B 35 (1987) 3679.
[91] A.P. Malozemoff, J. Appl. Phys. 63 (1988) 3874.
[92] A.P. Malozemoff, Phys. Rev. B 37 (1988) 7673.
[93] N.C. Koon, Phys. Rev. Lett. 78 (1997) 4865.
[94] T.C. Schulthess, W.H. Butler, Phys. Rev. Lett. 81 (1998) 4516.
[95] D.C. Khan, R.A. Erickson, J. Phys. Chem. Solids 29 (1968) 2087.